A superconducting diplexer for cosmic microwave background experiments

M. Madi, M. Mattes, J.R. Mosig, D. Rauly, P. Febvre

A Superconducting Diplexer for Cosmic Microwave Background Experiments

M Madi[1], M Mattes[1], J R Mosig[1], D Rauly[2], P Febvre[3]

1 Laboratory of Electromagnetics and Acoustics (LEMA), Swiss Federal Institute of Technology (EPFL), Lausanne, Switzerland
2 IMEP-LAHC, CNRS UMR5130, Grenoble, France
3 IMEP-LAHC, CNRS UMR5130, University of Savoie, Le Bourget du Lac, France

E-mail: mohammadreza.madi@epfl.ch, pascal.febvre@univ-savoie.fr

Abstract. Cosmic Microwave Background (CMB)‡ studies require observations in several frequency bands simultaneously. For example, the detection of clusters of remote galaxies can be performed by comparing CMB photon fluxes at different frequencies, using the spectral deformation of the Planck law, due to the Sunayev-Zeldovich effect. We propose a single pixel design to receive and detect simultaneously two frequency bands of the CMB, centered at 150 GHz and 220 GHz. It is composed of a bow-tie antenna, sensitive to the polarization of the incident radiation, feeding a diplexer structure to separate the signal towards two Kinetic Inductance Resonators associated respectively to the 130-170 and 200-270 GHz frequency bands. The diplexer makes use of 150 nm-thick Niobium-based superconducting transmission lines of Coplanar Strip-lines (CPS) type, for filtering and separation purposes, deposited on a 30 μm-thick Quartz substrate. A new coplanar matching structure, taking into account the kinetic inductance of the superconducting films, is proposed and achieves a nearly perfect match over more than 25% of each frequency band, along with a signal separation ratio above 30 dB at both center frequencies. The size of a single pixel is 0.9 mm $\times$ 1.2 mm.

‡ In cosmology, cosmic microwave background (CMB) radiation is thermal radiation filling the universe almost uniformly and it is explained as radiation left over from an early stage in the development of the universe [1]. The CMB radiation has a thermal black body spectrum at a temperature of 2.725 K, thus the spectrum peaks in the microwave range frequency of 160.2 GHz, corresponding to a 1.9 mm wavelength. This holds if you measure the intensity per unit frequency, as in Planck's law. If instead you measure it per unit wavelength, using Wien's law, the peak will be at 1.06 mm corresponding to a frequency of 283 GHz [2].

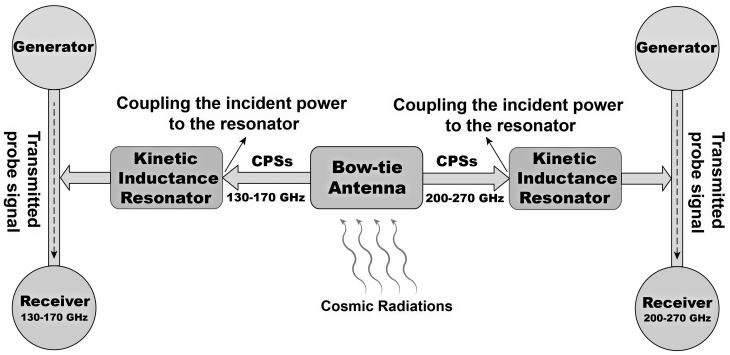

Figure 1. Sketch of the dual-band MKID detector under study.

1. Introduction

The development of fully integrated detectors for applications in astronomy, nuclear detection, atmospheric monitoring, or fundamental physics is nowadays of great attention. For example, two astronomical applications of these detectors concern the cartography of distant galaxies and clusters, and the measurement of B-modes § in the Cosmic Microwave Background. Cartography provides critical knowledge for understanding the origin and large-scale structures of the Universe [4]. High-precision measurement of the CMB is expected to confirm the existence of intense primordial gravitational waves and would provide the first and only observational evidence of the Cosmic Inflation phase. These observations require instruments with large focal planes, filled with detector arrays that efficiently absorb electromagnetic radiations [2].

The classical design of detector arrays is currently at its limit with respect to both pixel count and complexity of fabrication. The goal of this paper is to extend research towards superconducting resonant detectors. These sensors are simple to fabricate and are suitable for frequency multiplexing, which allows parallel readout of complex detector arrays. One solution, introduced in [5], is a single pixel design, to be included in an array in a next step, that receives and detects simultaneously two frequency bands of the CMB, centered respectively at 150 GHz and 220 GHz. It uses planar broadband antennas integrated on-chip with RF filters consisting of CoPlanar Strip-lines (CPS) and Broadside Coupled lines (BCL) [5]. However, the design proposed in [5] is narrow band and is not able to cover the desired atmospheric windows.

2. Dual-band MKID detector

In this work, we introduce a new configuration of a broadband frequency selective diplexer integrated with a Microwave Kinetic Inductance Detector (MKID) structure

§ Any polarization field can be decomposed into curl-free (E-mode) components, and pure curl components, called B-modes by analogy with electric and magnetic fields. The B-type harmonic modes exhibit linear polarization at $\pm 45°$ to the direction of modulation. The presence of B-modes in the CMB would be the distinctive signature of gravitational effects [3].

that covers the two atmospheric windows in the 130-170 GHz and 200-270 GHz frequency bands. The choice of the instrument frequency bands is motivated by antenna and atmospheric constraints.

MKID [6] is a superconducting microwave resonator, consisting of a lithographically defined strip of metal in close proximity with a high-frequency transmission line. The resonator has a geometry-dependent inductance and capacitance, as well as an intrinsic resistance, which damps the resonator [10]. Figure 1 depicts the set-up of the integrated MKID detector. To drive the two-band MKID shown in Figure 1, a microwave probe signal traveling through the transmission line is loaded by the MKID resonator at the resonance frequency. Off resonance, the probe signal will remain unaffected by the presence of the resonator. This simple arrangement is in fact a powerful detector since the resonant frequency depends sensitively upon both the surrounding environment and the internal superconducting dynamics. Since the total amount of inductance is the sum of geometrical and kinetic inductances (see section 3), a small change in either one of these will produce a significant change in the amplitude and phase of the transmitted probe signal.

This work focuses on the signal separation in the wide frequency band of interest. The diplexer is made of carefully chosen transmission lines of CPS type, since they have a high characteristic impedance and are easier to match to the antenna. A proper physical topology for the diplexer structure (antenna and CPS) is investigated considering the concept of complex surface impedance used in the Sonnet software‖.

3. Surface impedance and kinetic inductance

The tangential component E_t of the electric field of an ideal conductor is zero at its surface. Moreover, a current flows in a thin layer at the surface, as required to support the magnetic field H_t tangential to the surface. This short-circuit boundary condition excludes all fields from the interior of the ideal conductor [8]. In a real normal conductor, fields extend into the conductor decreasing exponentially with distance from the surface. The typical depth of penetration is well known as the skin depth [8]

$$\delta = (2/\omega\sigma\mu)^{1/2}, \tag{1}$$

where ω is the angular frequency of the surface currents, σ is the conductivity of conductor and μ is the absolute magnetic permeability of the conductor. To avoid the complication of solving Maxwell's equations inside conductors, the surface impedance

$$Z_s = E_t/H_t \tag{2}$$

is introduced providing the boundary condition for fields at the surface of the conductor, and accounts for the dissipation and energy stored inside the conductor [8]. The surface impedance for a normal conductor is [8],

$$Z_s = (1 + \mathrm{i})(\omega\mu/2\sigma)^{1/2} \tag{3}$$

‖ Sonnet is a Planar Electromagnetic Field Solver Software for High Frequency EM Simulation [7].

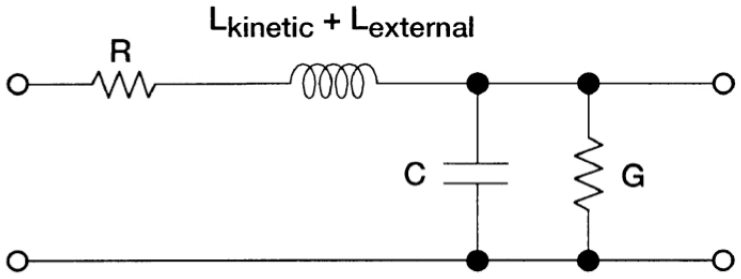

Figure 2. Lumped element equivalent circuit model for an incremental section of a superconducting transmission line [10].

and includes a resistive and an inductive term. The same formalism applies to superconductors. At a frequency well below the superconducting energy gap frequency, the conductivity σ is purely imaginary and is related to the London penetration depth λ_L that is independent of frequency [9]. For instance for Niobium at $\approx$ 4 K, and frequencies well below 700 GHz, $\lambda_L \approx 85$ nm. The surface impedance $Z_s = \mathrm{i}\omega\mu_0\lambda_L$ in the unit of Ω/square (where square indicates the unit of surface area) corresponds to a surface inductance $L_s = \mu_0\lambda_L$ in H/square (e.g. $L_s \approx 0.13$ pH/square, giving $Z_s \approx \mathrm{i}0.08$ Ω/square at 100 GHz) [8].

In circuit theory, the purely positive imaginary surface impedance corresponds to an extra inductance called kinetic inductance. Consequently, the total series inductance per unit length of a superconducting transmission line, L, consists of two parts, namely the internal inductance or the kinetic inductance per unit length, $L_{kinetic}$, which accounts for magnetic energy storage within the conductor, and the external inductance per unit length (depending on the geometry of the circuit), $L_{external}$ or $L_{geometry}$, which accounts for magnetic energy storage external to the conductor [10]:

$$L = L_{external} + L_{kinetic} \tag{4}$$

Figure 2 shows an equivalent circuit model for an incremental section of a superconducting transmission line. The kinetic inductance originates from the inertia of the paired carriers in the superconductor, while the external inductance arises from flux linkages. The kinetic inductance can be extracted from the surface impedance, with $Z_s = \mathrm{i}\omega L_{kinetic}$. Electromagnetic simulators can provide very accurate solutions for microwave circuits with ideal conductors. When the conductors are non-ideal, accurate results may still be obtained in many cases by specifying material parameters or surface impedances [8]. It has been shown that either a single thin sheet with the appropriate surface impedance, or a parallel pair of thin sheets separated by the thickness of the actual superconductor, can replace a thick superconductor [8]. Matick [11] has shown that the surface impedance seen by a plane wave normally incident on a conductor is the same as that seen by a wave traveling parallel to the conductor, as in a transmission line. A modified value of surface impedance can be used to correct the discrepancy between the real conductor and the two-sheet model. For superconductors,

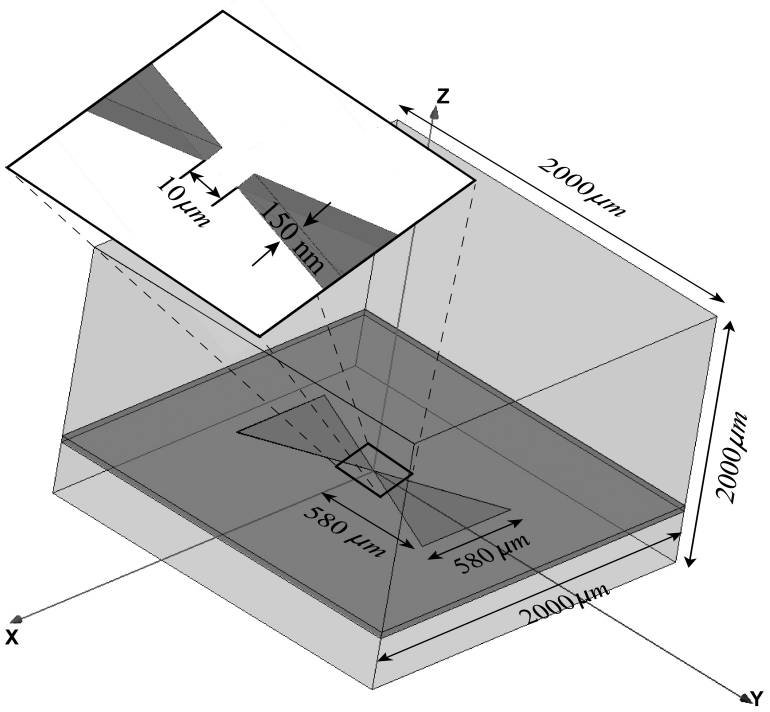

Figure 3. Geometry of the bow-tie antenna under study. The Niobium superconducting layer is 150 nm-thick, deposited over a 30 μm-thick Silicon substrate.

a simple correction to the surface impedance by introducing the β and coth factors [8] substantially improves the accuracy. It has been shown that the most accurate solution for simulating superconductors of finite thickness is obtained by replacing them with two thin conducting sheets whose surface impedance is $Z_s = \mathrm{i}\omega\mu_0\lambda_L \coth(t/\lambda_L)\beta$ [8]. The coth coefficient appears in the surface impedance of the single thin sheet, replacing the superconductor of finite thickness t, when the thickness t is not much greater than the London penetration depth λ_L [8]. On the other hand, the β coefficient adapts the surface impedance for the parallel pair of thin sheets replacing the single thick superconductor sheet [8]. It has been understood that by accepting a $\pm 2\%$ error margin in the characteristic impedance, the single thin sheet whose surface impedance is $Z_s = \mathrm{i}\omega\mu_0\lambda_L \coth(t/\lambda_L)$, is sufficient in our case to account for the single superconductor thick sheet. Consequently, we used the single thin sheet model, with coth correction only, for all simulations performed in this work.

4. Antenna design

Inspired by the design in [5], the proposed antenna is a Niobium bow-tie antenna deposited on a 30 μm-thick Silicon substrate, with a reflector back plane located 300 μm below the antenna plane (see Figure 3). The resistivity of the Silicon substrate is higher than 1000 Ω.cm. Niobium is typically sputtered with a DC power of 2.5 kW at a rate of about $30 - 40$ nm/min. The antenna is patterned via Reactive Ion Etching after

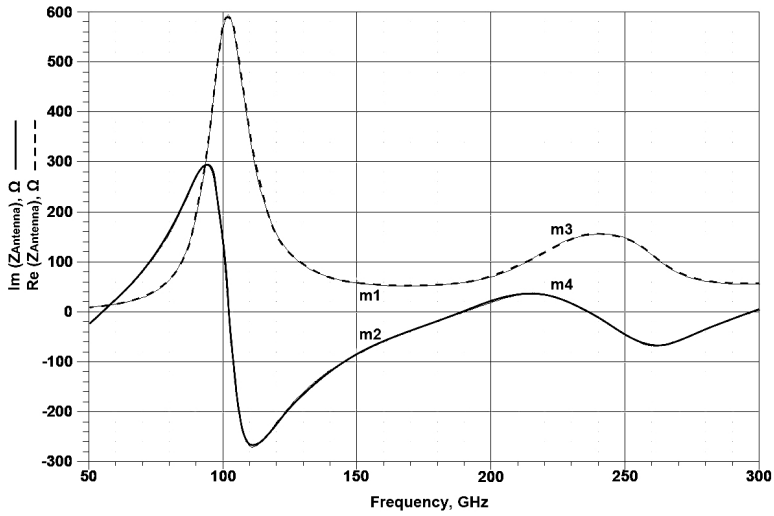

Figure 4. Antenna complex impedance in the frequency band of interest: **m1** (57.5 Ω at 150 GHz), **m2** (-85.5 Ω at 150 GHz), **m3** (120.7 Ω at 220 GHz) and **m4** (35.0 Ω at 220 GHz)

a resist deposition through optical lithography. The superconducting metallization is assumed to be 150 nm-thick. Open radiation type boundaries have been defined in the Sonnet electromagnetic simulator for the surrounding cubic box of 2000 μm side. The bow-tie antenna has been chosen because it has wideband characteristics. The antenna consists of two isosceles triangles whose bases and heights are equally 580 μm. The gap between two triangles of the antenna is 10 μm in order to directly connect it to CPSs. Figure 4 shows the real and imaginary part of the antenna impedance, seen from the 10 μm gap. It exhibits an out of band resonance at 100 GHz. The antenna impedance is $Z_{ant} = 57.5 - \mathrm{i}85.5\ \Omega$ at 150 GHz and $Z_{ant} = 120.7 + \mathrm{i}35.0\ \Omega$ at 220 GHz. Consequently, the diplexer structure studied in Section 5 must be designed to deliver the complex conjugate of the antenna impedance for optimal microwave power matching.

5. Diplexer design

Kinetic Inductance Resonators, shown in Figure 1, are assumed to have an input impedance of 200 Ω. The 200 Ω corresponds to the input impedance of a bolometer which has been introduced in [5]. In the new design, it is assumed that the bolometers are replaced by Kinetic Inductance Resonators of similar input impedance. Nevertheless, the use of different resonator impedance is straightforward and does not modify the proposed design; only the characteristic impedance of the quarter-wave transformer lines (TL3 and TL6 in Figure 5) needs to be changed. Two approaches are considered in order to deliver the highest amount of power to the 200 Ω loads in the two central frequencies of 150 GHz (left-side of antenna in Figure 1) and 220 GHz (right-side of antenna in Figure 1). The first design approach is an impedance matching using an appropriate length of transmission line, while the second approach is based on an impedance matching with

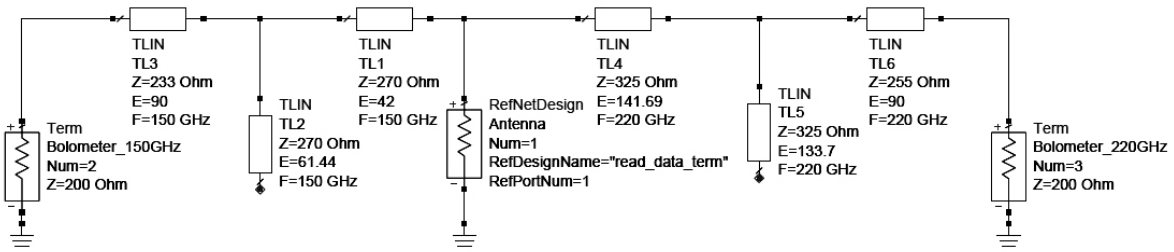

Figure 5. Schematics of the diplexer structure used in ADS [12]. It consists of transmission lines of the matching network coupled with the antenna whose frequency-dependent impedance is imported from HFSS. Impedances and electrical lengths of each part of the structure are mentioned for the center frequency.

a single-stub tuner.

In the first approach, using the Smith Chart, a proper length of transmission line is selected in order to transform the antenna complex impedance to a real impedance. The resulting real impedance is matched to the 200 Ω load using a Chebyshev two-section matching network, which is thereafter replaced by a single-section quarter-wave transformer (TL3 and TL6 in Figure 5) to reduce the dimension of the matching network, at the price of a narrower bandwidth. The characteristic impedance of the quarter-wave transformer is the geometric mean of the Chebyshev ones. The impedance matching procedure is done step-by-step employing the Smith Chart. The final analysis showed that the transmission coefficient in the band of interest is lowered by -1.2 dB, which means that part of the received power is lost in the diplexer by impedance mismatch, since the superconducting lines have no RF losses at the frequencies of interest. Moreover, a relatively low 6.5 dB signal separation ratio has been found between the two bands, which is associated to the risk of measuring part of the signal of one band in the other band of interest.

Consequently, we moved to a second approach that employs a single-shunt stub to match the antenna impedance to a real impedance. A short or an open circuit normally terminates the transmission line realizing the stub. An open circuit stub is chosen because it is more practical for fabrication in our case. The final configuration of the matching network is shown in Figure 5 from the ADS circuit representation¶. TL1 (resp. TL4) and TL2 (resp. TL5) are sections of the single-shunt stub matching network for each band of the diplexer. The antenna complex impedance is imported in ADS from the data obtained in HFSS$^+$ (Figure 4).

The transmission and reflection coefficients of the detector structure are displayed in Figure 6 and Figure 7. S_{21} and S_{31} are the transmission coefficients from the antenna to the left- and right-side, respectively, of the structure shown in Figure 1. Port 1 is the

¶ Advanced Design System (ADS) is an electronic design automation software system from Agilent EEsof EDA, a unit of *Agilent Technologies* [12].

$^+$ High Frequency Structural Simulator (HFSS) is a commercial finite element method solver for electromagnetic structures from Ansys [13].

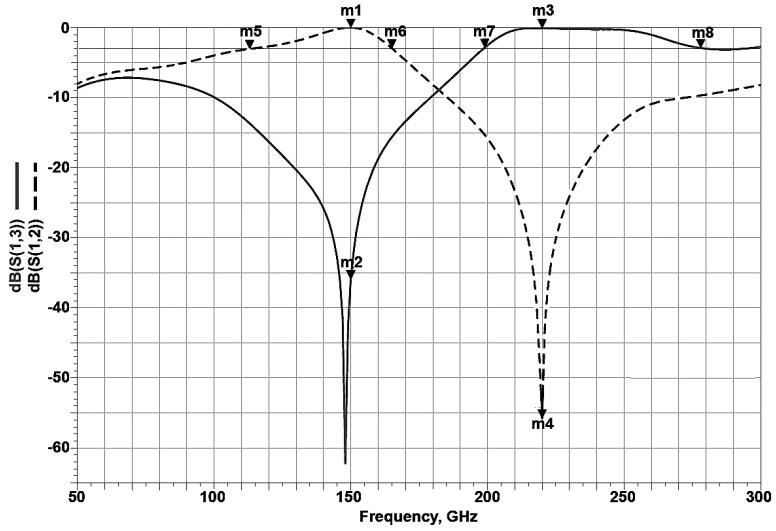

Figure 6. Antenna transmission coefficients from the left- (S_{21}) and right-side (S_{31}) of the detector structure (in dB). Port 1 is the RF input port of the antenna. The measured points: **m1** ($S_{21} = -0.007$ dB at 150 GHz), **m2** ($S_{31} = -36.0$ dB at 150 GHz), **m3** ($S_{31} = -0.1$ dB at 220 GHz), **m4** ($S_{21} = -56.0$ dB at 220 GHz), **m5** ($S_{21} = -3.0$ dB at 113 GHz), **m6** ($S_{21} = -3.0$ dB at 165 GHz), **m7** ($S_{31} = -3.0$ dB at 199 GHz) and **m8** ($S_{31} = -3.0$ dB at 278 GHz)

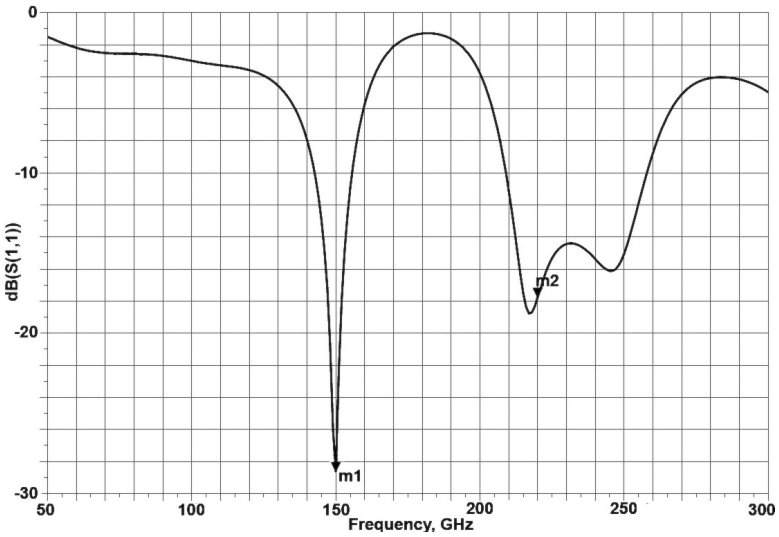

Figure 7. Reflection coefficient (S_{11}) of the detector structure seen from the antenna port. The measured points: **m1** ($S_{11} = -29.0$ dB at 150 GHz) and **m2** ($S_{11} = -18.0$ dB at 220 GHz).

RF input port of the antenna. It is seen that the detector exhibits less than 3 dB of signal attenuation in each of the two bands, as well as an excellent signal separation of up to 35 dB at their central frequencies.

Table 1. Physical dimensions of transmission lines with $\lambda_L = 85$ nm

	Length (μm)	s (μm)	w (μm)
CPS TL1	140	10	1.7
CPS TL2	178	2	0.6
CPS TL3	308	10	2.7
CPS TL4	318	10	1
CPS TL5	268	5	0.6
CPS TL6	86	10	2.1

6. Diplexer topology and layout

The diplexer design is based on the electrical length and characteristic impedance of each section of the detector of Figure 5. All transmission lines are assumed to be of CPS type and the thickness t of the metallization is 150 nm. A trade-off between Quartz and Silicon substrate shows an improvement of $\sim 25\%$ in transmission coefficient in the central frequency and $\sim 30\%$ improvement in bandwidth by using the Quartz substrate ($\epsilon_r = 3.78$). Though the pixel size stays the same in both cases, to investigate the best performance of the structure, the diplexer is considered to be fabricated on 30 μm Quartz substrate. The London penetration depth is 85 nm for Niobium. The width of strips w and the gap s between them are defined in an iterative algorithm, from a proper primary guess. The CPS effective magnetic permeability μ_{eff} and effective dielectric constant ϵ_{eff} are derived from the analytical solutions of [14, 15]. These parameters, which are a function of the London penetration depth of the Niobium superconductor and of geometrical factors (width of strips, gap between strips and thickness of metallization), allow us to calculate the characteristic impedance of the CPS lines. The kinetic inductance of CPS in H/square is given in [14]:

$$L_{kinetic} = \mu_0 \lambda_L \coth[t/(2\lambda_L)] \tag{5}$$

For instance, choosing $s = 10$ μm and $w = 1.7$ μm for TL1 gives $\mu_{eff} = 1.03$ and $\epsilon_{eff} = 2.34$, which results in a characteristic impedance of about 270 Ω. The electrical length of TL1 is 42 degrees or $0.166\lambda_g$ at 150 GHz where the guided wavelength is $\lambda_g = \lambda_0/(\epsilon_{eff}\mu_{eff})^{1/2}$; λ_0 is the wavelength in free space that is approximately 2 mm at 150 GHz. The length of TL1 shall therefore be 148 μm. The kinetic inductance of CPS with the thickness $t = 150$ nm, and $\lambda_L = 85$ nm, is around 0.15 pH/square. This value was inserted in Sonnet for the strips. The length of TL1 was optimized at 140 μm to be compatible with ADS simulation results.

The final dimensions of all transmission lines are listed in Table 1. The topology of Figure 8, including the coupling between all branches (e.g. impact of TL2 on TL3), is properly taken into account in Sonnet simulation. The antenna complex impedance is obtained as well from HFSS simulations. The whole structure is then simulated from an electrical point of view with ADS. The transmission and reflection coefficients of the

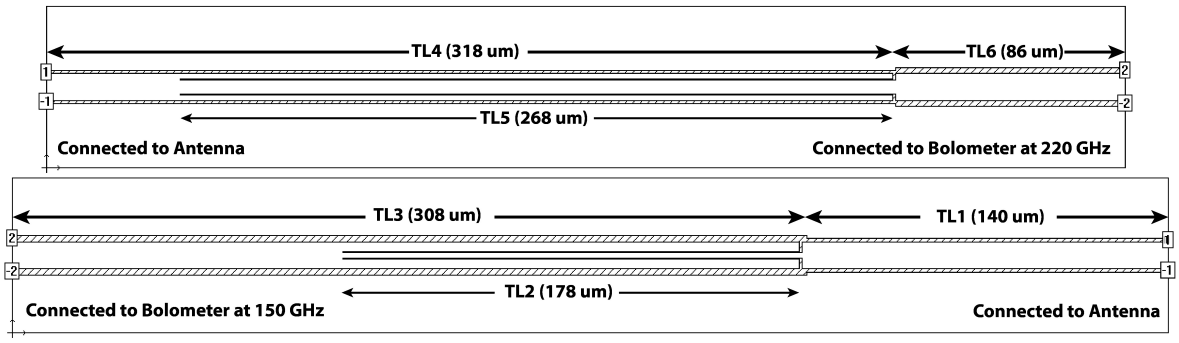

Figure 8. Top: right-side structure designed for 200-270 GHz with TL5 stub inserted within TL4. Bottom: TL2 shunt is placed between two strips of TL3 in the left-side structure designed for 130-170 GHz.

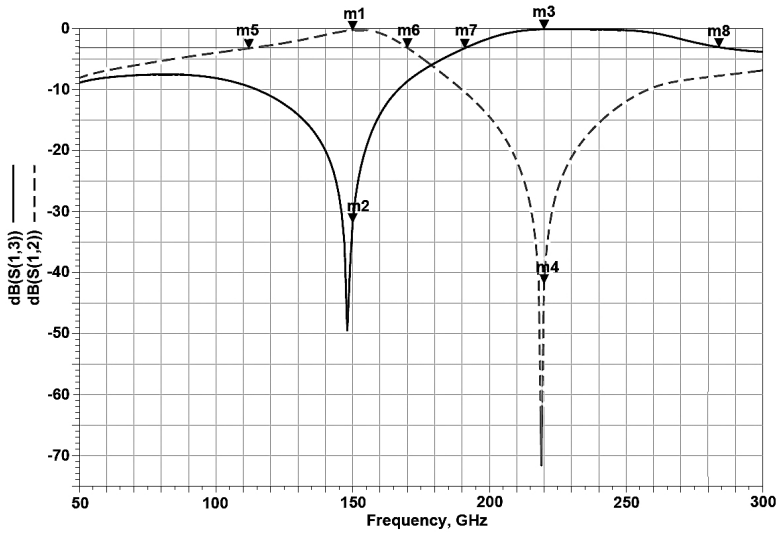

Figure 9. Transmission coefficients from antenna to 150 GHz (S_{21}) and 220 GHz (S_{31}) detector loads, for the proposed topology of Figure 8. The measured points: **m1** ($S_{21} = -0.3$ dB at 150 GHz), **m2** ($S_{31} = -32.0$ dB at 150 GHz), **m3** ($S_{31} = -0.1$ dB at 220 GHz), **m4** ($S_{21} = -42.0$ dB at 220 GHz), **m5** ($S_{21} = -3.3$ dB at 112 GHz), **m6** ($S_{21} = -3.2$ dB at 170 GHz), **m7** ($S_{31} = -3.2$ dB at 191 GHz) and **m8** ($S_{31} = -3.1$ dB at 284 GHz)

proposed topology are displayed respectively in Figure 9 and Figure 10.

7. Conclusion

The design of a broadband 130–170 GHz and 200–270 GHz detection structure, with pixel-size of 0.9 mm $\times$ 1.2 mm and more than 30 dB signal-separation ratio at the central frequencies of 150 GHz and 220 GHz requirements, has been achieved. It requires rigorous modeling of the superconducting transmission lines. The method proposed in this paper could be applied to other structures for similar applications. Furthermore, a new topology for parallel CPS shunts embedded in CPS transmission lines was proposed

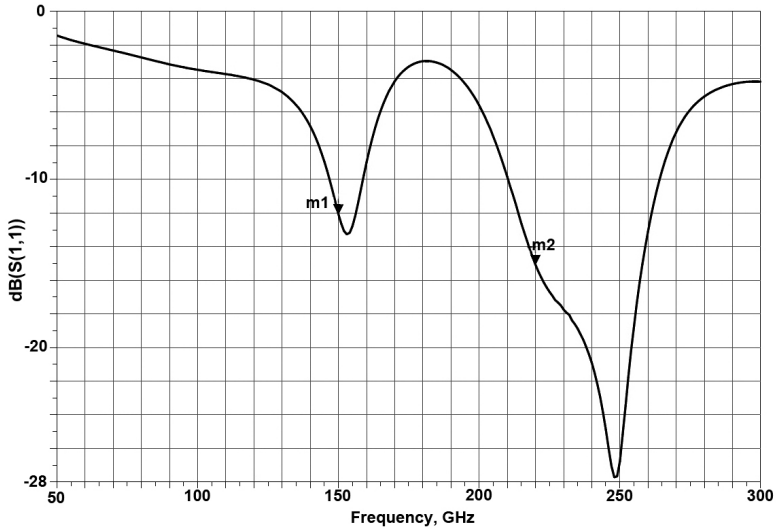

Figure 10. Reflection coefficient (S_{11}) of the proposed topology seen from the antenna port. The meassured points: **m1** ($S_{11} = -12.1$ dB at 150 GHz) and **m2** ($S_{11} = -15.1$ dB at 220 GHz).

and demonstrates promising results that fit the requirements.

Acknowledgments

This work has been partially funded by the MKIDS project of the French ANR research agency. A. Monfardini and C. Hoffmann are gratefully acknowledged for providing scientific input to this work.

References

[1] Penzias A A and Wilson R W 1965 *Astrophys. J.* **142** 419–21
[2] Fixsen D J 2009 *Astrophys. J.* **707** 916–920
[3] Carlstrom J E, Kovac J, Leitch E M and Pryke C 2003 *New Astron. Rev.* **47** 953–66
[4] Nati F *et al* 2007 *New Astron. Rev.* **51** 385–9
[5] Rauly D *et al* 2008 *Piers Online* **4**, 671–5.
[6] Day P K *et al* 2003 *Nature* **425** 817–21
[7] Sonnet home page:http://www.sonnetsoftware.com/
[8] Kerr A R 1999 *MMA Memo* vol 245
[9] Tinkham M 1975 *Introduction to Superconductivity* (New York: McGraw-Hill)
[10] Rainee N 2001 *Coplanar Waveguide Circuits, Components, and Systems* (John Wiley & Sons, Inc.)
[11] Matick R E 1969 *Transmission Lines for Digital and Communication Networks* (New York: McGraw-Hill)
[12] ADS home page: http://www.home.agilent.com/
[13] Ansys home page: http://www.ansys.com
[14] Febvre P *et al* 1995 *Millimeter and Submillimeter Waves II Proc. SPIE* **2558** 136–47
[15] Gupta K C *et al* 1979 *Microstrip lines and slotlines* (Boston, MA:Artech House Publishers) chapter 7